IEEE Access
Multidisciplinary | Rapid Review | Open Access Journal

Received 1 April 2024, accepted 21 April 2024, date of publication 30 April 2024, date of current version 7 May 2024.

Digital Object Identifier 10.1109/ACCESS.2024.3395301

RESEARCH ARTICLE

Impacts of Co-Channel Interference on Performance of Downlink IRS-NOMA Systems

THAI-ANH NGUYEN[1], HOANG-VIET NGUYEN[1], DINH-THUAN DO[2], (Senior Member, IEEE), AND BYUNG MOO LEE[3,4], (Senior Member, IEEE)

[1]Faculty of Electronics Technology, Industrial University of Ho Chi Minh City, Ho Chi Minh City 700000, Vietnam
[2]School of Engineering, University of Mount Union, Alliance, OH 44601, USA
[3]Department of Intelligent Mechatronics Engineering, Sejong University, Seoul 05006, South Korea
[4]Department of Convergence Engineering for Intelligent Drone, Sejong University, Seoul 05006, South Korea

Corresponding author: Byung Moo Lee (blee@sejong.ac.kr)

This work was supported in part by the Basic Science Research Program through the National Research Foundation of Korea (NRF) funded by Korean Government Ministry of Science and ICT (MSIT) under Grant NRF-2023R1A2C1002656; in part by MSIT, South Korea, (ICT Challenge and Advanced Network of HRD Program) under Grant IITP-2024-RS-2022-00156345; and in part by the Faculty Research Fund of Sejong University, in 2024.

ABSTRACT Recently, intelligent reflective surface (IRS)-aided systems are becoming a prospective technology in realizing for sixth generation (6G) wireless communication era because of extremely low power transmission, seamless coverage and their superiority. These network systems can allow many users and devices to connect to each other, extending the coverage. To empower IRS-aided systems, non-orthogonal multiple access (NOMA) can be leveraged to work with IRS technique enabling further benefits such as mass connectivity, flexible resource allocation and improved performance. Increasing connected devices and expanding coverage means devices have the potential to interfere with each other. Recent studies focusing on researching and analyzing the performance of the IRS-supported NOMA network have not taken into account or not fully calculated the impact of interference on system performance. In this study, we first analyze the effect of co-channel interference (CCI) at users in downlink IRS-NOMA systems. In particular, the CCIs generated by the terminals deployed randomly in the coverage area affect the signal reception at the user in the downlink. In this network model, the channel conditions that follow the Rayleigh distribution and the CCI statistical model are independent and identically distributed. We analyze and evaluate network performance by extracting closed-form expressions of outage probability, ergodic capacity, total achievable rate then highlighting the adverse effects of CCI on IRS-NOMA. In addition, to improve the performance of the IRS-NOMA downlink, we present a framework of theorical analysis to look more insights of users' performance, i.e. diversity order. Our analytical derivatives are verified through computer simulations based on Monte-Carlo and intuitive comparisons with the benchmarks.

INDEX TERMS Intelligent reflecting surface, non-orthogonal multiple access, outage probability, ergodic rate, co-channel interference.

NOMENCLATURE

AWGN	Additive white Gaussian noise.
B5G	Beyond fifth generation.
6G	Sixth generation.
BER	Bit error rate.
BPSK	Binary phase shift keying.
BS	Base station.
CDF	Cumulative density function.
CCI	Co-channel interference.
CSI	Channel state information.
IRS	Intelligent reflecting surfaces.

The associate editor coordinating the review of this manuscript and approving it for publication was Zesong Fei.

IoT	Internet-of-things.
UAV	Unmanned aerial vehicle.
MIMO	Multi-input-multi-output.
NOMA	Non-orthogonal multiple access.
OMA	Orthogonal Multiple Access.
OP	Outage probability.
PDF	Probability distribution density.
SIC	Successive interference cancellation.
UE	User.
ER	Ergodic rate.

I. INTRODUCTION

In the era of wireless communications, speed, capacity, and stable connectivity are the most important aspects to achieve hyper-connectivity. With the tremendous support of their predecessors, next generation wireless networks are about to revolutionize communications in a wide range of fields such as artificial intelligence, edge computing, sensing technologies, internet-of-things (IoT), virtual and augmented realities, and many more futuristic applications [1], [2], [3], [4]. However, along with the exponential increase in the evolution of technologies, the day-to-day requirements of wireless system evolution are also increasing, like unlimited spectrum requirements, advanced connectivity. To achieve these possibilities, various kinds of research are being suggested. The recent techniques such as IRS [5] and NOMA [6] are such developments in the field of wireless systems.

NOMA has been one of the most promising techniques in the field of wireless communication since the evolution of such access technique allows multiple users to acquire the same time and frequency slots, exploiting the power domain, and allocating different power levels to distinguish at the receiver [6]. NOMA offers important advantages such as improved spectral efficiency, user fairness, and system capacity. In [7], the non-regenerative massive-MIMO-NOMA relay systems were introduced here to enhance the system SE and further enlarge the coverage range. The authors used the MMSE-SIC decoding method to decode the received information. The system capacity and sum rate were addressed by the closed-form expressions with the help of matrix theories. Research has demonstrated that the number of transmitting antennas and the number of users have a positive but decreasing correlation with system performance and total speed. However, deploying the MIMO-NOMA system requires expensive costs, complex techniques, and in some complex terrain areas it is difficult to deploy effectively.

Meanwhile, IRS is a device made up of multiple tiny-size programmable meta-surface elements inserted on a plane surface which has the capacity to reflect, refract, or scatter incoming electromagnetic waves in a controlled manner. The scope of the IRS is its deployment ability in any position or place as per the requirements since it is a small and plane device. By adjusting the phase, amplitude, and polarization of the reflected signals, IRS can optimize the wireless channel and overcome signal propagation challenges such as path loss, interference, and multipath fading. With their ability to shape and steer signals, IRS offers several advantages including increased signal strength, extended coverage, enhanced energy efficiency, and improved quality of service.

A. RELATED WORK

In [8], [9], and [10], the authors presented an extensive survey of the current state of NOMA research, including its key concepts, advantages, and applications. They also delved into various aspects of NOMA system design, such as power allocation, user pairing, and interference management techniques. Additionally, the article identifies and discusses several open research challenges in NOMA, including resource allocation optimization, user fairness, and scalability issues. Meanwhile in [9], the authors discussed the motivation behind NOMA, highlighting its ability to increase system capacity and spectral efficiency compared to conventional orthogonal multiple access schemes. They provided a detailed overview of the NOMA concept, including its key principles, such as power domain multiplexing and successive interference cancellation. The paper also investigates the performance of NOMA through simulations, demonstrating its advantages in terms of user fairness, coverage, and capacity enhancement. Furthermore, the authors discuss potential challenges and open research issues associated with NOMA, paving the way for further investigations and advancements in this area. In [10], the authors examined the impact of imperfect channel state information (CSI) on the system performance and evaluates the achievable rate and error probability. The paper provides insights into the design and optimization of NOMA systems under realistic channel information assumptions. Meanwhile, in [12], the authors addressed the issue of user fairness in decode-forward relaying NOMA schemes with imperfect successive interference cancellation (SIC) and CSI. It considers a relay-assisted NOMA system and proposes an improved user fairness scheme that accounts for imperfect SIC and CSI at the relay. The paper presented performance evaluations and simulations to demonstrate the effectiveness of the proposed scheme in achieving fairness among users. In [11], the authors addressed the challenge of achieving fairness among users in a NOMA system and propose a fairness index based on the achievable rates of users. The paper considered a fairness-aware resource allocation scheme that aims to improve fairness among users while maintaining high system performance. In [13], the authors study the impact of imperfect CSI. This is due to channel estimation errors and feedback delays as well as imperfect sequential noise cancellation on the performance of uplink NOMA networks with randomly deployed mobile terminals. The results of the study show that estimation errors reduce the coding gain for low SNR. However, the degradation effect of channel estimation error on uplink NOMA becomes negligible when SNR is high. Additionally, the results also depict that the

feedback delay does not negatively affect the uplink NOMA for low SNR. However, it reduces the coding gain for high SNR and the imperfect successive denoising and ordering of the decoding process results in a loss of coding gain for high SNR. In [14], the authors studied the adverse effects of randomly deployed CCI interference communicating over NOMA on the performance of an uplink network supporting half/duplex relaying and amplification. Among them, non-orthogonal CCI affected the relay and BS reception. The authors calculated the system performance parameters and confirmed that the lagrange multiplier optimization technique was used to optimize the location of the relay, the transmitted power and the power allocation factor for NOMA. The results show that non-orthogonal CCI seriously degrades the system performance.

In [15], the authors focused on scenarios to highlight benefits of IRS, which also results in challenging situation for ensuring secure communications. The authors proposed an IRS-assisted transmission scheme that utilizes the reflective properties of the intelligent surfaces to enhance the secrecy rate. By intelligently adjusting the phase shifts of the IRS elements, the proposed scheme aims to optimize the signal alignment at the legitimate receiver while creating intentional interference at the eavesdropper. The paper provides theoretical analyses and simulations to demonstrate the effectiveness of the proposed scheme in achieving secure and confidential communication in scenarios where the eavesdropper's CSI is not known. In [16], the authors focused on two key aspects: passive beamforming and deployment design of the IRS. The authors proposed a passive beamforming strategy for the IRS to maximize the received signal power at the intended destination while suppressing self-interference. By carefully adjusting the phase shifts of the IRS elements, the proposed strategy aims to achieve enhanced signal reception at the destination and improved cancellation of self-interference in full-duplex communication. Additionally, the paper addresses the deployment design of the IRS by considering factors such as the placement of the IRS and the number of elements. The authors provide theoretical analysis and simulations to evaluate the performance of the proposed strategies in terms of signal-to-interference-plus-noise ratio and capacity. In [17], the authors proposed an IRS-assisted interference mitigation scheme where the IRS elements are strategically deployed to enhance the signal quality at the unmanned aerial vehicle (UAV) and suppress interference to the ground users. The proposed scheme utilizes the passive beamforming capabilities of the IRS to enhance the received signal power at the UAVs while minimizing interference to the ground users. The paper provides theoretical analyses and simulations to demonstrate the effectiveness of the IRS-assisted interference mitigation scheme in improving the system performance in terms of signal-to-interference-plus-noise ratio and outage probability. In [18], the authors investigated the utilization of intelligent reflecting surfaces (IRS) in multiple access systems with user pairing, specifically comparing the performance of NOMA and Orthogonal Multiple Access (OMA) schemes. The paper explores the question of whether NOMA or OMA should be employed in IRS-assisted multiple-access scenarios. The authors propose a framework that considers user pairing and power allocation strategies for both NOMA and OMA. They evaluate the system performance in terms of achievable rates and user fairness under different scenarios. The paper provides insights into the benefits and trade-offs of NOMA and OMA in IRS-assisted multiple access systems and identifies the conditions under which each scheme can offer advantages. In [19], the authors focus on securing NOMA networks against eavesdropping attacks by leveraging the reflective properties of the IRS. The authors propose a secure transmission scheme that optimizes the beamforming at the transmitter, the phase shifts at the IRS, and the power allocation among NOMA users. By strategically adjusting the IRS phase shifts, the proposed scheme aims to create intentional signal cancellation at the eavesdroppers, while ensuring reliable communication with legitimate users. The paper provides theoretical analysis and simulations to evaluate the secrecy rate and system performance in terms of secure communication.

In [20], the authors investigated the use of IRS to enhance the secrecy performance in NOMA systems by optimizing the beamforming and power allocation strategies. The authors propose a secure transmission scheme that considers both legitimate users and potential eavesdroppers. They analyzed the secrecy outage probability and derive analytical expressions for the secrecy rate. Meanwhile, in [21], the authors explored the use of multiple distributed IRSs to improve the security of NOMA communications. The authors propose a secure transmission scheme that optimizes the IRS phase shifts and power allocation among NOMA users. By strategically adjusting the IRSs, the scheme aims to create intentional interference at potential eavesdroppers, while ensuring reliable communication with the intended recipients. These articles contribute to the understanding and advancement of secure NOMA networks by leveraging intelligent reflecting surfaces. They highlight the potential of IRS in enhancing the physical layer security of NOMA systems, providing insights into the design and optimization of secure transmission schemes for wireless communication systems. In the work [23], the authors study the impact of CCI on the leakage rate of NOMA networks in the power-domain supported by illegal relays. The analysis results show that since invalid forwarding is affected by a limited number of friendly jammers and CCI jammers, its achieved rate is low and saturates at high SNR. The results also show that CCI causes a loss in system coding gain on user outage performance. In the work [24], the authors study imperfect CSI caused by channel estimation errors and feedback delay effects in leakage rate analysis for cooperative NOMA networks. The results show that the channel estimation error causes system coding gain loss while the feedback delay does not have any effect on the user's OP at the untrusted

relay terminal in the mode low SNR. Conversely, the channel estimation error effects become negligible while the feedback delay causes system coding gain losses to the user's OP at the untrusted relay terminal at high SNR. However, recent studies focusing on analyzing the performance of IRS-NOMA systems have not considered or have not fully calculated the effect of nearby devices or systems. Therefore, it could be necessary to look at the impacts of interference on the IRS-NOMA systems' performance.

B. MOTIVATIONS AND OUR CONTRIBUTIONS

The impacts of CCI could be crucial problem in design of wireless networks, and its consideration in the analysis and design of such systems is necessary because of the reuse of frequency channels to improve spectrum efficiency. In this paper, we emphasize on a IRS-NOMA network model at the downlink. Considering the users affected by the CCI are identical and we rely on the proposed model to re-examine mathematical expressions for the performance parameters of the system and thereby evaluate the system performance. The detailed system model and the system performance metrics can be listed as follows:

- We propose a model of IRS-NOMA system in downlink mode, with CCI affected at users. We construct the probability distribution density function (PDF) and cumulative probability distribution (CDF) expressions of the new channel model, considering the number of IRS reflective elements and if the links between the base station (BS) to the IRS and the IRS link to the user (UE) are possible links with a Rayleigh fading distribution.[1]
- Next, we calculate the instantaneous and average SINR at the users of the system, derive low complexity closed-form expressions for the outage probability (OP) and ergodic rate (ER) of the system.
- Finally, we simulate to prove and verify between theory and analysis. The simulation results show the superiority of the IRS at higher IRS meta-surface elements.

A comparison of our work with other related papers is also presented in Table 1. In addition, our main contributions are summarized as follows:

- We evaluate the performance of the IRS-NOMA system when subjected to CCI at users with different amounts of interference. We analyze the impact of CCI on the performance of the IRS-NOMA system when the power allocation coefficients of NOMA are changed.
- We derive expressions to achieve explicit system performance analysis, i.e. OP and ER for UEs for IRS-NOMA system which can be fairly compared with the benchmark namely IRS-OMA system. We also compute diversity order to look insights the system performance.
- To confirm the superiority of IRS, we compare the performance of the IRS-NOMA system and the benchmark (IRS-OMA system) with the influence of CCI. The expected performance is illustrated through simulations to conclude that the number of CCI source, number of meta-surface elements at IRS, power distribution coefficients are considered as the main parameters that make crucial impacts on the system performance.

[1]The Rayleigh fading model has become the basic analytically tractable model which produces initial analysis and important insights into IRS-NOMA systems. There have been many research projects applying the fading Rayleigh model, such as [33], [34], and [35] and references therein. This assumption stems from the fact that even if the line of sight links between BS-IRS and IRS-UE are blocked, widespread dispersion still exists.

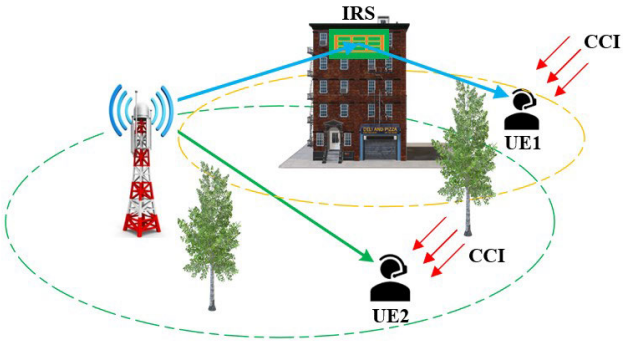

FIGURE 1. System model.

C. ORGANIZATION AND NOTATIONS

The rest of the paper is organized as follows. Section II presents IRS-NOMA network model in downlink under the impact of CCI. Section III examines some distribution of related channels. Section IV presents analysis of system performance. Numerical results and discussion are presented in Section V. Finally, Section VI. concludes the paper.

The main notations of this paper are as follows: $\Pr(.)$ denotes the probability operator; $\mathrm{E}[.]$ denotes the expectation operator; $f_X(.)$ and $F_X(.)$ denote the PDF and the CDF, respectively; $CN(.,.)$ is a circularly symmetric complex Gaussian distribution; and $\sim$ stands for "distributed as"; $|.|$ is absolute operator; $\mathrm{Ei}(.)$ denotes the exponential integral function [27, Eq. (8.211.1)]. An identity matrix of size $M \times M$ is denoted by I_M; $(.)^H$ denotes the conjugate and Hermitian transpose; a diagonal matrix with $s_1, \ldots, s_M$ on the diagonal is denoted by $diag(s_1, \ldots, s_M)$. $\Gamma(\cdot)$ is the gamma function, and $\gamma(\cdot,\cdot)$ is the lower incomplete gamma function.

II. IRS-NOMA SYSTEM MODEL UNDER THE IMPACT OF CCI

We investigate the IRS-NOMA network model in downlink mode under CCI at UEs. Specifically, the BS has single antenna to communicate with groups of single antenna users. In this scenario, we just analyze performance of a user pair including UE1, UE2, where these users are exposed to multiple identical CCI. The BS communicates directly with UE2 without IRS support, at UE2 there is the impact of many

TABLE 1. Comparison of the our paper with similar studies.

Content	Our Scheme	[29]	[30]	[31]	[32]
Comparison of IRS-NOMA and IRS-OMA system performance with the impact of CCI	x	x	x	x	x
Analyze system performance with different numbers of CCI	x	x	x	x	x
Analyze system performance with different numbers of IRS elements	x				
Analyze system performance with different IRS-NOMA power allocation factors	x				
Outage probability	x	x	x	x	x
Ergodic Rate	x	x	x		
System throughput	x	x			
Diversity order	x				

identical CCI, shown in Fig. 1.[2] Assume that the number of CCI disturbances at UE1 and UE2 are the same and there are M CCI sources. In addition, the distance between each CCI signal to UE1 and UE2 is equal to 1. IRS has N_x metasurface elements and IRS has its reflecting matrix defined theoretically as $\Theta = diag(\beta_1 e^{j\theta_1}, \beta_2 e^{j\theta_2}, \ldots, \beta_{N_x} e^{j\theta_{N_x}})$, $j = \sqrt{-1}$, where $\beta_k \in [0,1]$ is the reflectance amplitude and $\theta_k \in [0,2\pi)$ is the phase shift of the k-th element that can be adjusted by IRS ($k = 1, 2, \ldots, K$).

A. ANALYSIS OF CHANNEL MODEL

Considering the BS-IRS-UE1 channel, it is assumed that all channels are flat fading channels while the BS knows the complete CSI. In particular, the receivers at IRS-NOMA system can estimate the channel to obtain an accurate CSI. The BS-IRS and IRS-UE links can be LoS or NLoS for different cases. The channel parameter between the BS and the IRS is the same, denoted $G_{IRS} \in C^{1\times N_x}$. The channel parameter between the IRS and the UEs is the same, denoted $g_{UE1} \in C^{N_x\times 1}$. They are represented as vector spaces $G_{IRS} = [G_1, G_2, \ldots, G_{N_x}]$ and $g_{UE1} = [g_1, g_2, \ldots, g_{N_x}]^T$, respectively. All elements in G_{IRS} and g_{UE1} follow a Rayleigh fading distribution CN (0, 1). In a BS-UE2 link, assuming a flat fading channel, and at a BS with complete CSI, the G_U channel gain follows a Rayleigh fading distribution, $G_U \sim CN$ (0, 1). At all UEs affected by M sources of CCI, the CCI channel coefficient is $h_{I,i}$ with ($i = 1, \ldots, M$). The CCIs all have a statistically independent Rayleigh fading model CN (0, 1). Therefore, the UEs are influenced by the sum of M CCI sources that are statistically independent and have a Rayleigh fading distribution $\gamma_I = \sum_{i=1}^{M} P_{I,i}|h_{I,i}|^2$, where $P_{I,i}$ is the i-th CCI noise power. According to [22] the PDF function of the sum of M sources of CCI terms that is statistically independent and has a Rayleigh fading distribution which is determined as follows:[3]

$$f_{\gamma_I}(y) = \frac{y^{M-1}}{(P_I\Omega_I)^M (M-1)!} exp\left(\frac{-y}{P_I\Omega_I}\right), \quad (1)$$

where $\Omega_I = E[h_{I,i}^2]$, $P_I = P_{I,i}$.[4]

B. ANALYSIS OF SIGNALS AT DOWNLINK

The transmitted signal of the BS is represented as

$$x = \sqrt{\alpha_1 P_s} s_{UE1} + \sqrt{\alpha_2 P_s} s_{UE2}, \quad (2)$$

where, P_s is the transmit power at the BS; s_{UE1}, s_{UE2} are the signals that the BS transmits to UE1 and UE2, respectively; α_1, α_2 are called the power allocation factors of the BS sending signals to UE1, UE2, respectively. The α_1 and α_2 parameters satisfy the condition $\alpha_1 + \alpha_2 = 1$. Assuming that UE1 is affected by M sources of CCI, and similar for UE2. The signal received at the UEs can be represented as follows:

The received signal at UE1 is given by

$$y_{UE1} = \left(G_{IRS}\Theta g_{UE1} d_{IRS}^{-\frac{\alpha_{G_{IRS}}}{2}} d_{UE1}^{-\frac{\alpha_{g_{UE1}}}{2}}\right) x + \sum_{i=1}^{M} \sqrt{P_{I,i}} h_{I,i} s_I + n_{UE1}. \quad (3)$$

The received signal at UE2 is given by

$$y_{UE2} = \left(G_{UE2} d_{UE2}^{-\frac{\alpha_{G_{UE2}}}{2}}\right) x + \sum_{i=1}^{M} \sqrt{P_{I,i}} h_{I,i} s_I + n_{UE2}, \quad (4)$$

where d_{IRS} is the distance from BS to IRS, d_{UE1} is the distance from IRS to UE1, d_{UE2} is the distance from BS to UE2, n_{UE1} is defined as Gaussian noise at UE1, n_{UE2} is defined as Gaussian noise at UE2, n_{UE1} and n_{UE2} has the same variance as σ^2. It is assumed that $n_{UE1}^2 = n_{UE2}^2 = 1$.

[2]To improve system performance, we can cluster users, where users are divided into multiple groups and NOMA is deployed in each group, and different groups are allocated orthogonal bandwidth resources. By adopting user grouping, the complexity of receiver design is reduced and the problem of error propagation caused by SIC is also alleviated [36], [37]. We leave such a design and its analysis as interesting future work.

[3]In the NOMA downlink network with CCI action at the UEs, the CCIs are considered i.i.d. and i.n.i.d. [29]. There is still loss of generality in our model considering only CCI as i.i.d.

[4]In practice, UEs are affected by CCIs with different capacities. However, the assumption that they have the same maximum transmit power is still valid as described in recent 5G specifications [38]. We therefore denote as the maximum transmit power of the CCI terminals.

C. SIGNAL-TO-INTERFERENCE-PLUS-NOISE RATIO AT THE UES

Signal-to-interference-plus-noise ratio (SINR) is defined as the ratio of the average effective signal power divided by the average noise power plus the average noise power. Therefore, the SINR at the UEs is determined as follows:

At UE1, the s_{UE2} signal is treated as a noise signal, then we have a SINR at UE1:

$$SINR_{UE1} = \frac{\gamma_S \alpha_1}{\gamma_S \alpha_2 + \gamma_I + 1}. \quad (5)$$

At UE2, the s_{UE1} signal is treated as a noise signal, then we have a SINR at UE2:

$$SINR_{UE2} = \frac{\gamma_U \alpha_2}{\gamma_U \alpha_1 + \gamma_I + 1}, \quad (6)$$

where $\gamma_S = |G_{IRS}\Theta g_{UE1}|^2 d_{IRS}^{-\alpha_{G_{IRS}}} d_{UE1}^{-\alpha_{g_{UE1}}} P_S$; $\gamma_U = |G_{UE2}|^2 d_{UE2}^{-\alpha_{G_{UE2}}} P_S$; $\gamma_I = \sum_{i=1}^{M_{I,i}} P_{I,i} |h_{I,i}|^2$.

III. THE CHANNELS' STATISTICS

In this section we calculate the statistics of the system channels.

A. THE IRS'S PARAMETERS

Assume the quality of the BS-IRS-UE channel is best for the UE users. To do this, one can adjust the parameters of the IRS so that it is optimal. That is, we maximize $|G_{IRS}\Theta g_{UE1}| = \left| \sum_{k=1}^{N_x} \beta_k G_{IRS,k} g_{UE1,k} e^{j\theta_k} \right|$, where $G_{IRS,k}$ and $g_{UE1,k}$ is the k-th element of G_{IRS} and g_{UE1} respectively. This can be achieved by intelligently adjusting the θ_k phase shift for each element, that is, the phases of all $G_{IRS,k} g_{UE1,k} e^{j\theta_k}$ are set the same. After applying the optimal $\{\theta_k\}$ [25], $\beta_k = \beta$, we have:

$$|G_{IRS}\Theta g_{UE1}|^2 = \beta^2 \left(\sum_{k=1}^{N_x} |G_{IRS,k}| \, |g_{UE1,k}| \right)^2. \quad (7)$$

B. THE CHANNEL STATISTICS

We construct the closed-form expressions CDF and PDF for random variable $X = \sum_{k=1}^{N_x} |G_{IRS,k}| \, |g_{UE1,k}|$, where $|G_{IRS,k}|$, $|g_{UE1,k}|$ are two random variables with Rayleigh distribution with variance of 1 and statistically independent. Since $|G_{IRS,k}|$, $|g_{UE1,k}|$ are two random variables with Rayleigh distribution, the product $|G_{IRS,k}| \, |g_{UE1,k}|$ is also a random variable with a double Rayleigh distribution. The result X is the sum of N_x random variables with statistically independent double Rayleigh distribution, according to [26]. The PDF function and the CDF function of X can be approximated as the first term of the Laguerre series expansion defined as follows:

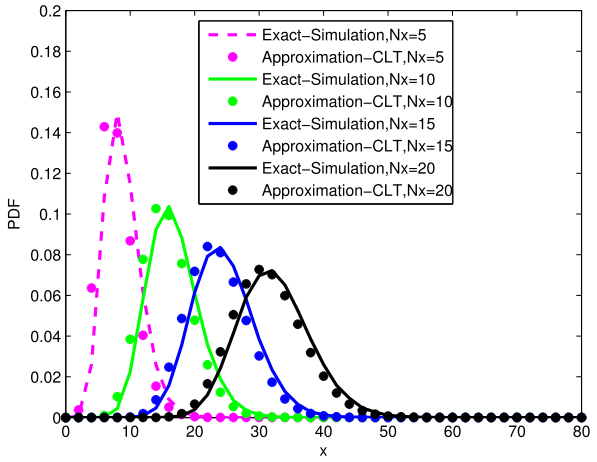

FIGURE 2. PDF function of X with different number of IRS reflectance elements.

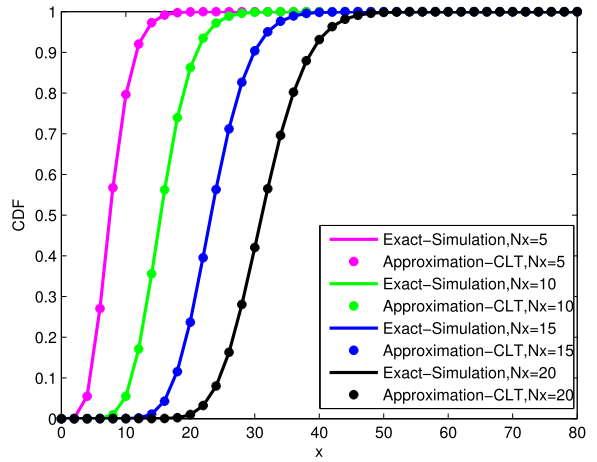

FIGURE 3. CDF function of X with different number of IRS reflectance elements.

$$f_X(x) = \frac{x^a}{b^{a+1}\Gamma(a+1)} exp\left(-\frac{x}{b}\right), \quad (8)$$

$$F_X(x) = \frac{\gamma\left(a+1, \frac{x}{b}\right)}{\Gamma(a+1)}, \quad (9)$$

where $a = \frac{\Omega_1^2}{\Omega_2} - 1$, $b = \frac{\Omega_2}{\Omega_1}$, with $\Omega_1 = \mathrm{E}[X]$ and $\Omega_2 = 4Var[X]$.

Using the Monte-Carlo simulation method by Matlab software with the number of different N_x reflector elements of the IRS, We can simulate the PDF and CDF as follows (Fig. 2, Fig. 3)

Theorem 1: Let X be the sum of N_x random variables with a statistically independent double Rayleigh distribution. The expectation and variance of X are determined as follows:

$$\mathrm{E}[X] = \frac{N_x \pi}{2} \quad (10)$$

$$Var[X] = N_x \left(1 - \frac{\pi^2}{16}\right) \quad (11)$$

Proof: Please refer to Appendix I

Theorem 2: Given the random variable $\gamma_S = \beta^2\left(\sum_{k=1}^{N_x}\left|G_{IRS,k}\right|\left|g_{UE1,k}\right|\right)^2 d_{IRS}^{-\alpha_{G_{IRS}}} d_{UE1}^{-\alpha_{g_{UE1}}} P_S$, the PDF and CDF functions of γ_S are defined as follows:

$$f_{\gamma_S}(y) = \frac{y^{\frac{a-1}{2}}}{2b^{a+1}\Gamma(a+1)\, n^{\frac{a+1}{2}}} exp\left(-\frac{1}{b}\sqrt{\frac{y}{n}}\right), \quad (12)$$

$$F_{\gamma_S}(y) = \frac{\gamma\left(a+1, \frac{1}{b}\sqrt{\frac{y}{n}}\right)}{\Gamma(a+1)}, \quad (13)$$

where $n = \beta^2 d_{IRS}^{-\alpha_{G_{IRS}}} d_{UE1}^{-\alpha_{g_{UE1}}} P_S$.

Proof: Please refer to Appendix II

Theorem 3: Given a random variable γ_S then the expectation of $E[\gamma_S]$ and $E\left[\gamma_S^2\right]$ is determined as follows:

$$E[\gamma_S] = \frac{b^2 n\Gamma(a+3)}{\Gamma(a+1)}, \quad (14)$$

$$E\left[\gamma_S^2\right] = \frac{b^4 n^2\Gamma(a+5)}{\Gamma(a+1)}, \quad (15)$$

where $a = \frac{N_x\pi^2}{16-\pi^2} - 1$, and $b = \frac{16-\pi^2}{2\pi}$.

Proof: Please refer to Appendix III

Theorem 4: Given the random variable $\gamma_U = |G_{UE2}|^2 d_{UE2}^{-\alpha_{G_{UE2}}} P_S$, the PDF and CDF functions of γ_U are defined as follows:

$$f_{\gamma_U}(y) = \frac{1}{2m} exp\left(-\frac{y}{2m}\right), \quad (16)$$

$$F_{\gamma_U}(y) = 1 - exp\left(-\frac{y}{2m}\right), \quad (17)$$

where $m = d_{UE2}^{-\alpha_{G_{UE2}}} P_S$.

Proof: Please refer to Appendix IV

Theorem 5: Given a random variable γ_U then the expectation of $E[\gamma_U]$ and $E\left[\gamma_U^2\right]$ is determined as follows:

$$E[\gamma_U] = 2m, \quad (18)$$

$$E\left[\gamma_U^2\right] = 2!(2m)^2. \quad (19)$$

Proof: Please refer to Appendix V

Theorem 6: Given a random variable γ_I then the expectation of $E[\gamma_I]$ and $E\left[\gamma_I^2\right]$ is determined as follows:

$$E[\gamma_I] = MP_I\Omega_I, \quad (20)$$

$$E\left[\gamma_I^2\right] = M(M+1)(P_I\Omega_I)^2. \quad (21)$$

Proof: Please refer to Appendix VI

IV. SYSTEM PERFORMANCE ANALYSIS

In this section, we calculate the downlink IRS-NOMA network performance parameters with the impact of CCI interference at the UEs.

A. OUTAGE PROBABILITY

The OP is an important parameter commonly used to measure the performance of a wireless system. The OPs of UE1 and UE2 are calculated as follows:

For UE1, the OP is given by

$$OP_{UE1} = \Pr(SINR_{UE1} < \gamma_{th}). \quad (22)$$

Substituting (5) into (22), we get

$$OP_{UE1} = \Pr\left(\frac{\gamma_S\alpha_1}{\gamma_S\alpha_2 + \gamma_I + 1} < \gamma_{th}\right). \quad (23)$$

We can transform (23) to get (24)

$$OP_{UE1} = \Pr\left(\gamma_S < \frac{\gamma_{th}(\gamma_I+1)}{\alpha_1 - \gamma_{th}\alpha_2}\right). \quad (24)$$

Set $\gamma_{thS} = \frac{\gamma_{th}}{\alpha_1-\gamma_{th}\alpha_2}$, by applying statistical probability theory, we have

$$OP_{UE1} = \int_0^\infty F_{\gamma_S}(\gamma_{thS}(y+1)) f_{\gamma_I}(y)\, dy. \quad (25)$$

Substituting (13) into (25), we get

$$OP_{UE1} = \frac{\int_0^\infty \gamma\left(a+1, \sqrt{\frac{\gamma_{thS}(y+1)}{nb^2}}\right) f_{\gamma_I}(y)\, dy}{\Gamma(a+1)}. \quad (26)$$

Set $t = 1 - 2exp(-y)$, which leads to $dy = \frac{1}{1-t}dt$, and perform the simple mathematical transformation, we get

$$OP_{UE1} = \int_{-1}^{1} \frac{P_{UE1}(t) f_{\gamma_I}\left(\ln\left(\frac{2}{1-t}\right)\right)}{(1-t)} dt, \quad (27)$$

where $P_{UE1}(t) = \frac{\gamma\left(a+1, \sqrt{\frac{\gamma_{thS}\left(\ln\left(\frac{2}{1-t}\right)+1\right)}{nb^2}}\right)}{\Gamma(a+1)}$. Using the Chebyshev-Gauss quadrture integration method, we can calculate OP_{UE1}:

$$OP_{UE1} = \sum_{i=1}^{L} \frac{\varpi_i P_{UE1}(t_i) f_{\gamma_I}\left(\ln\left(\frac{2}{1-t_i}\right)\right)\sqrt{1-t_i^2}}{1-t_i}, \quad (28)$$

where $\varpi_i = \frac{\pi}{L}$, $t_i = cos\frac{(2i-1)\pi}{2L}$.

We consider the OP of UE1 at high SNR. The transmit SNR is $\rho = \frac{P_S}{\sigma^2}$. At high SNR: when $\rho \to \infty$ then $F_{\gamma_S}(y)$ can be approximated as follows [39]

$$F_{\gamma_S}(y) = \frac{\gamma\left(a+1, \frac{1}{b}\sqrt{\frac{y}{n}}\right)}{\Gamma(a+1)} \approx \frac{\left(\frac{1}{b}\sqrt{\frac{y}{n}}\right)^{a+1}}{\Gamma(a+1)}. \quad (29)$$

Theorem 7: When $\rho \to \infty$ then OP_{UE1}^{∞} is determined as follows:

$$OP_{UE1}^{\infty} = \frac{\left(\frac{1}{b}\sqrt{\frac{\gamma_{th}}{(\alpha_1-\gamma_{th}\alpha_2)n}}\right)^{a+1} exp\left(\frac{1}{P_I\Omega_I}\right)}{\Gamma(a+1)(P_I\Omega_I)^M(M-1)!} M_2, \quad (30)$$

where M_2 can be obtained by

$$M_2 = (-1)^j \sum_{j=0}^{M-1} \left[C_{M-1}^{j} \left(\frac{1}{P_I \Omega_I} \right)^{-(e-j)} \Gamma\left(e-j, \frac{1}{P_I \Omega_I} \right) \right], \tag{31}$$

where $e = \frac{a+1}{2} + M$.

Proof: Please refer to Appendix A

For UE2, the OP is given by

$$OP_{UE2} = \Pr\left(SINR_{UE2} < \gamma_{th} \right). \tag{32}$$

Substituting (6) into (29) we get

$$OP_{UE2} = \Pr\left(\frac{\gamma_U \alpha_2}{\gamma_U \alpha_1 + \gamma_I + 1} < \gamma_{th} \right). \tag{33}$$

Transform (30) to get (31)

$$OP_{UE2} = \Pr\left(\gamma_U < \frac{\gamma_{th}\left(\gamma_I + 1\right)}{\alpha_2 - \gamma_{th}\alpha_1} \right). \tag{34}$$

Set $\gamma_{thU} = \frac{\gamma_{th}}{\alpha_2 - \gamma_{th}\alpha_1}$.

Applying statistical probability theory to the channel model with CCI noise, we have

$$OP_{UE2} = \int_0^{\infty} F_{\gamma_U}\left(\gamma_{thU}\left(y+1\right)\right) f_{\gamma_I}\left(y\right) \mathrm{d}y. \tag{35}$$

Substituting (1) and (17) into (32) we get

$$OP_{UE2} = \frac{\int_0^{\infty} P_{UE2}\left(y\right) y^{M-1} exp\left(\frac{-y}{P_I \Omega_I}\right) \mathrm{d}y}{\left(P_I \Omega_I\right)^M \left(M-1\right)!}, \tag{36}$$

where $P_{UE2}\left(y\right) = y^{M-1}\left(1 - exp\left(-\frac{\gamma_{thU}\left(y+1\right)}{2m}\right)\right)$.

Transform (33) to get (34)

$$OP_{UE2} = 1 - B\int_0^{\infty} \left(y^{M-1} exp\left(-Cy\right) \right) \mathrm{d}y, \tag{37}$$

where $B = \frac{exp\left(-\frac{\gamma_{thU}}{2m}\right)}{\left(P_I \Omega_I\right)^M \left(M-1\right)!}$, $C = \frac{\gamma_{thU}}{2m} + \frac{1}{P_I \Omega_I}$.

Using [27, eq 3.351], we have

$$OP_{UE2} = 1 - B\left(M-1\right)! C^{-M}. \tag{38}$$

We consider the OP of UE2 at high SNR. The transmit SNR is $\rho = \frac{P_S}{\sigma^2}$. At high SNR: When $\rho \to \infty$, $F_{\gamma_U}\left(y\right)$ can be approximated as follows [29]

$$F_{\gamma_U}\left(y\right) = 1 - exp\left(-\frac{y}{2m}\right) \approx \frac{y}{2m}. \tag{39}$$

Theorem 8: When $\rho \to \infty$ then OP_{UE2}^{∞} is determined as follows:

$$OP_{UE2}^{\infty} = \frac{\gamma_{th}\left[M\left(M+1\right)\left(P_I \Omega_I\right)^2 + 1\right]}{2m\left(\alpha_2 - \gamma_{th}\alpha_1\right)}. \tag{40}$$

Proof: Please refer to Appendix B

B. DIVERSITY ORDER

The diversity order is a crucial performance measurement used to evaluate OP's attenuation under the impact of transmit SNR at the transmitter. In the principle, the diversity order refers to a quantity asymptotically as the SNR goes to infinity. The diversity order is defined as

$$D_{UE} = -\frac{\partial \log\left(OP_{UE}^{\infty}\right)}{\partial \log \rho} = -\frac{\rho}{OP_{UE}^{\infty}} \frac{\partial OP_{UE}^{\infty}\left(\rho\right)}{\partial \rho}. \tag{41}$$

For UE1:

$$D_{UE1} = -\frac{\rho}{OP_{UE1}^{\infty}} \frac{\partial OP_{UE1}^{\infty}\left(\rho\right)}{\partial \rho}. \tag{42}$$

Set $\lambda_{UE1} = \frac{1}{b}\sqrt{\frac{\gamma_{th}}{\left(\alpha_1 - \gamma_{th}\alpha_2\right)\beta^2 d_{IRS}^{-\alpha_{G_{IRS}}} d_{UE1}^{-\alpha_{g_{UE1}}}}}$, D_{UE1} is defined as

$$D_{UE1} = -\frac{\rho}{\left(\frac{\lambda_{UE1}}{\sqrt{\rho}}\right)^{a+1}} \frac{\partial\left(\left(\frac{\lambda_{UE1}}{\sqrt{\rho}}\right)^{a+1}\right)}{\partial \rho}. \tag{43}$$

So we can determine D_{UE1} as follows

$$D_{UE1} = \frac{a+1}{2}. \tag{44}$$

For UE2:

$$D_{UE2} = -\frac{\rho}{OP_{UE2}^{\infty}} \frac{\partial OP_{UE2}^{\infty}\left(\rho\right)}{\partial \rho}. \tag{45}$$

Set $\lambda_{UE2} = \frac{\gamma_{th}\left[M\left(M+1\right)\left(P_I \Omega_I\right)^2 + 1\right]}{2d_{UE2}^{-\alpha_{G_{UE2}}}\left(\alpha_2 - \gamma_{th}\alpha_1\right)}$, D_{UE2} is defined as

$$D_{UE2} = -\frac{\rho}{\frac{\lambda_{UE2}}{\rho}} \frac{\partial\left(\frac{\lambda_{UE2}}{\rho}\right)}{\partial \rho}. \tag{46}$$

So we can determine D_{UE2} as follows

$$D_{UE2} = 1. \tag{47}$$

C. ERGODIC RATE ANALYSIS

The ER is a parameter commonly used to analyze and evaluate the performance as added metric along with OP. The theoretical ERs of the respective UEs are calculated as follows:

$$R_{UE1} = \mathrm{E}\left(\log_2\left(1 + SINR_{UE1}\right)\right), \tag{48}$$

$$R_{UE2} = \mathrm{E}\left(\log_2\left(1 + SINR_{UE2}\right)\right). \tag{49}$$

We first consider ER analysis of the UE1.

Substituting (5) into (45), we have

$$R_{UE1} = \mathrm{E}\left[\log_2\left(1 + \frac{\gamma_S \alpha_1}{\gamma_S \alpha_2 + \gamma_I + 1}\right)\right]. \tag{50}$$

Transform (47) to get (48)

$$R_{UE1} = \mathrm{E}\left[\log_2\left(\frac{\gamma_S + \gamma_I + 1}{\gamma_S \alpha_2 + \gamma_I + 1}\right)\right]. \tag{51}$$

It is noted that

$$\mathrm{I}_1 = \mathrm{E}\left[\log_2\left(\gamma_S + \gamma_I + 1\right)\right], \tag{52}$$

$$\mathrm{I}_2 = \mathrm{E}\left[\log_2\left(\gamma_S\alpha_2 + \gamma_I + 1\right)\right]. \tag{53}$$

We have

$$R_{UE1} = I_1 - I_2. \tag{54}$$

We calculate I_1 via these steps.

Applying the calculation in [28], we can compute I_1

$$\mathrm{I}_1 = \frac{\ln\left(1 + E\left[\gamma_S + \gamma_I\right]\right)}{\ln 2} - \frac{E\left[(\gamma_S + \gamma_I)^2\right] - E^2\left[\gamma_S + \gamma_I\right]}{2(1 + E\left[\gamma_S + \gamma_I\right])^2 \ln 2}. \tag{55}$$

It is worth noting that γ_S and γ_I are random, statistically independent variables

$$\mathrm{I}_1 = \frac{\ln\left(1 + E\left[\gamma_S\right] + E\left[\gamma_I\right]\right)}{\ln 2} - \frac{E\left[\gamma_S^2\right] + E\left[\gamma_I^2\right] - E^2\left[\gamma_S\right] - E^2\left[\gamma_I\right]}{2(1 + E\left[\gamma_S\right] + E\left[\gamma_I\right])^2 \ln 2}. \tag{56}$$

Applying the results obtained above to (53), we have

$$\mathrm{I}_1 = \log_2\left(1 + \frac{nb^2\Gamma\left(a+3\right)}{\Gamma\left(a+1\right)} + MP_I\Omega_I\right) - \frac{\frac{b^4n^2\Gamma(a+5)}{\Gamma(a+1)} + M(P_I\Omega_I)^2 - \left(\frac{nb^2\Gamma(a+3)}{\Gamma(a+1)}\right)^2}{2\ln\left(2\right)\left(1 + \frac{nb^2\Gamma(a+3)}{\Gamma(a+1)} + MP_I\Omega_I\right)^2}. \tag{57}$$

By doing the same I_1, we calculate I_2

$$\mathrm{I}_2 = \frac{\ln\left(1 + \alpha_2 E\left[\gamma_S\right] + E\left[\gamma_I\right]\right)}{\ln 2} - \frac{\alpha_2^2 E\left[\gamma_S^2\right] + E\left[\gamma_I^2\right] - \alpha_2^2 E^2\left[\gamma_S\right] - E^2\left[\gamma_I\right]}{2(1 + \alpha_2 E\left[\gamma_S\right] + E\left[\gamma_I\right])^2 \ln 2}. \tag{58}$$

Applying the results obtained above to (55), we have

$$\mathrm{I}_2 = \log_2\left(1 + \alpha_2\frac{nb^2\Gamma\left(a+3\right)}{\Gamma\left(a+1\right)} + MP_I\Omega_I\right) - \frac{\frac{\alpha_2^2b^4n^2\Gamma(a+5)}{\Gamma(a+1)} + M(P_I\Omega_I)^2 - \alpha_2^2\left(\frac{nb^2\Gamma(a+3)}{\Gamma(a+1)}\right)^2}{2\ln\left(2\right)\left(1 + \alpha_2\frac{nb^2\Gamma(a+3)}{\Gamma(a+1)} + MP_I\Omega_I\right)^2}. \tag{59}$$

Comment 1: The saturated ER of UE1 reaches near the threshold of high SNR. Therefore, at high SNR, $\rho \to \infty$, applying the results of the work [39], we can approximate the ER of UE1 as follows: When $\rho \to \infty$, infer $\gamma_S \to \infty$, therefore R_{UE1}^{∞} is calculated

$$R_{UE1}^{\infty} = \log_2\left(1 + \lim_{\gamma_S\to\infty}\frac{\gamma_S\alpha_1}{\gamma_S\alpha_2 + \gamma_I + 1}\right). \tag{60}$$

Then, R_{UE1}^{∞} is computed by

$$R_{UE1}^{\infty} = \log_2\left(1 + \frac{\alpha_1}{\alpha_2}\right). \tag{61}$$

Now, we move on ER analysis of the UE2:

Substituting (6) into (46)

$$R_{UE2} = \mathrm{E}\left[\log_2\left(1 + \frac{\gamma_U\alpha_2}{\gamma_U\alpha_1 + \gamma_I + 1}\right)\right]. \tag{62}$$

By setting

$$T_1 = \mathrm{E}\left[\log_2\left(\gamma_U + \gamma_I + 1\right)\right]. \tag{63}$$

also setting

$$T_2 = \mathrm{E}\left[\log_2\left(\gamma_U\alpha_1 + \gamma_I + 1\right)\right]. \tag{64}$$

We have

$$R_{UE2} = T_1 - T_2. \tag{65}$$

By doing the same I_1, we calculate T_1 and T_2

$$T_1 = \frac{\ln\left(1 + 2m + MP_I\Omega_I\right)}{\ln 2} - \frac{(2m)^2 + M(P_I\Omega_I)^2}{2(1 + 2m + MP_I\Omega_I)^2\ln 2}, \tag{66}$$

$$T_2 = \frac{\ln\left(1 + 2\alpha_1 m + MP_I\Omega_I\right)}{\ln 2} - \frac{(2\alpha_1 m)^2 + M(P_I\Omega_I)^2}{2(1 + 2\alpha_1 m + MP_I\Omega_I)^2\ln 2}. \tag{67}$$

Comment 2: The saturated ER of UE2 reaches near the threshold of high SNR. Therefore, at high SNR, $\rho \to \infty$, applying the results of the work [39], we can approximate the ER of UE2 as follows: When $\rho \to \infty$, infer $\gamma_U \to \infty$, therefore R_{UE2}^{∞} is calculated

$$R_{UE2}^{\infty} = \log_2\left(1 + \lim_{\gamma_U\to\infty}\frac{\gamma_U\alpha_2}{\gamma_U\alpha_1 + \gamma_I + 1}\right). \tag{68}$$

Then, R_{UE2}^{∞} is computed by

$$R_{UE2}^{\infty} = \log_2\left(1 + \frac{\alpha_2}{\alpha_1}\right). \tag{69}$$

D. IRS-OMA PERFORMANCE PARAMETERS OF THE SAME MODEL

In this section we calculate the performance parameters of the IRS-OMA model with the impact of CCI interference at the UEs. Compare the performance between the IRS-NOMA system and the IRS-OMA system. We can consider OMA as a special case of NOMA. For a fair comparison we assume that each UE receives its resources the same as in the NOMA case. The SINR at UEs in OMA mode can be calculated as follows:

SINR at UE1 and UE2:

$$SINR_{UE1}^{OMA} = \frac{\gamma_S}{\gamma_I + 1}, \tag{70}$$

$$SINR_{UE2}^{OMA} = \frac{\gamma_U}{\gamma_I + 1}. \tag{71}$$

The OPs of UE1 and UE2 are calculated as follows:

Considering on UE1,

$$OP_{UE1}^{OMA} = \Pr\left(SINR_{UE1}^{OMA} < \gamma_{th}\right). \tag{72}$$

Transforming (69) we get (70)

$$OP_{UE1}^{OMA} = \Pr\left(\gamma_S < \gamma_{th}\left(\gamma_I + 1\right)\right). \tag{73}$$

We have

$$OP_{UE1}^{OMA} = \int_0^{\infty} F_{\gamma_S}\left(\gamma_{th}\left(y+1\right)\right) f_{\gamma_I}\left(y\right) \mathrm{d}y. \tag{74}$$

Transforming (71) we get (72)

$$OP_{UE1}^{OMA} = \frac{\int_0^{\infty} \gamma\left(a+1, \frac{1}{b}\sqrt{\frac{\gamma_{th}(y+1)}{n}}\right) f_{\gamma_I}\left(y\right) \mathrm{d}y}{\Gamma\left(a+1\right)}. \tag{75}$$

By similar calculation OP_{UE1}, OP_{UE1}^{OMA} is determined as follows

$$OP_{UE1}^{OMA} = \sum_{i=1}^{L} \frac{\varpi_i P_{UE1}^{OMA}\left(t_i\right) f_{\gamma_I}\left(\ln\left(\frac{2}{1-t_i}\right)\right)\sqrt{1-t_i^2}}{1-t_i}, \tag{76}$$

where $P_{UE1}^{OMA}\left(t_i\right) = \frac{\gamma\left(a+1, \sqrt{\frac{\gamma_{th}\left(\ln\left(\frac{2}{1-t_i}\right)+1\right)}{nb^2}}\right)}{\Gamma(a+1)}$.

At user UE2, we compute

$$OP_{UE2}^{OMA} = \Pr\left(SINR_{UE2}^{OMA} < \gamma_{th}\right). \tag{77}$$

Transform (74) to get (75)

$$OP_{UE2}^{OMA} = \Pr\left(\gamma_U < \gamma_{th}\left(\gamma_I + 1\right)\right). \tag{78}$$

Applying statistical probability theory, we have

$$OP_{UE2}^{OMA} = \int_0^{\infty} F_{\gamma_U}\left(\gamma_{th}\left(y+1\right)\right) f_{\gamma_I}\left(y\right) \mathrm{d}y. \tag{79}$$

By similar calculation OP_{UE2}, OP_{UE2}^{OMA} is determined as follows

$$OP_{UE2}^{OMA} = 1 - B_1\left(M-1\right)!\left(C_1\right)^{-M}, \tag{80}$$

where $B_1 = \frac{exp\left(-\frac{\gamma_{th}}{2m}\right)}{\left(P_I\Omega_I\right)^M (M-1)!}$ and $C_1 = \frac{\gamma_{th}}{2m} + \frac{1}{P_I\Omega_I}$.

The ERs of UE1 and UE2 are calculated as follows:

At user UE1, we compute The ER of UE1 is defined as follows:

$$R_{UE1}^{OMA} = \mathrm{E}\left(\log_2\left(1 + SINR_{UE1}^{OMA}\right)\right). \tag{81}$$

Substitute (67) into (78)

$$R_{UE1}^{OMA} = \mathrm{E}\left[\log_2\left(1 + \frac{\gamma_S}{\gamma_I + 1}\right)\right]. \tag{82}$$

Transform (79) to get (80)

$$R_{UE1}^{OMA} = \mathrm{E}\left[\log_2\left(\gamma_S + \gamma_I + 1\right)\right] - \mathrm{E}\left[\log_2\left(\gamma_I + 1\right)\right]. \tag{83}$$

Set $\mathrm{I}_1^{OMA} = \mathrm{E}\left[\log_2\left(\gamma_S + \gamma_I + 1\right)\right]$ and $\mathrm{I}_2^{OMA} = \mathrm{E}\left[\log_2\left(\gamma_I + 1\right)\right]$.

We have

$$R_{UE1}^{OMA} = I_1^{OMA} - I_2^{OMA}. \tag{84}$$

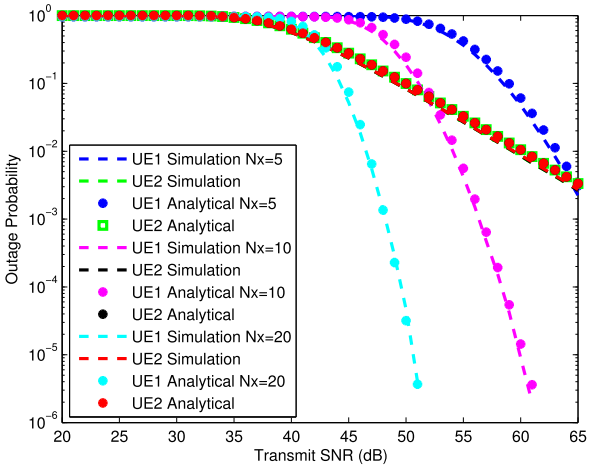

FIGURE 4. OPs of UEs with different IRS reflector numbers.

By similar calculation R_{UE1}, R_{UE1}^{OMA} is determined as follows

$$I_1^{OMA} = I_1, \tag{85}$$

$$\mathrm{I}_2^{OMA} = \frac{1}{\ln 2}\left[\ln\left(1 + MP_I\Omega_I\right) - \frac{M\left(P_I\Omega_I\right)^2}{2\left(1+MP_I\Omega_I\right)^2}\right]. \tag{86}$$

At user UE2, we compute The ER of UE2 is defined as follows:

$$R_{UE2}^{OMA} = \mathrm{E}\left(\log_2\left(1 + SINR_{UE2}^{OMA}\right)\right). \tag{87}$$

Substitute (68) into (84)

$$R_{UE2}^{OMA} = \mathrm{E}\left[\log_2\left(1 + \frac{\gamma_U}{\gamma_I + 1}\right)\right]. \tag{88}$$

Transform (85) to get (86)

$$R_{UE2}^{OMA} = \mathrm{E}\left[\log_2\left(\gamma_U + \gamma_I + 1\right) - \log_2\left(\gamma_I + 1\right)\right]. \tag{89}$$

Set $T_1^{OMA} = \mathrm{E}\left[\log_2\left(\gamma_U + \gamma_I + 1\right)\right]$ and $T_2^{OMA} = \mathrm{E}\left[\log_2\left(\gamma_I + 1\right)\right]$.

We have

$$R_{UE2}^{OMA} = T_1^{OMA} - T_2^{OMA}. \tag{90}$$

By doing similar calculations, R_{UE2} and R_{UE1}^{OMA}, R_{UE2}^{OMA} are determined as follows

$$T_1^{OMA} = T_1, \tag{91}$$

$$T_2^{OMA} = I_2^{OMA}. \tag{92}$$

V. SIMULATION RESULTS AND DISCUSSIONS

In this part, we simulate the OP, ER according to range of SR, using Monte Carlo simulation method on Matlab software to prove the correctness of the theory. The simulation settings are set as shown in Table 2.

In Fig. 4, we simulate the OPs of the UEs. In which, the number of IRS reflector elements is 5, 10, and 20 elements, respectively. In this mode, the power allocation factor for UE1 is 0.8, UE2 is 0.2. At UE1 and UE2 are affected by six CCI elements. Without loss of generality, we assume

TABLE 2. Simulation parameters [39].

No	Meaning	Parameters
1	Bandwidth	$B = 1Mhz$
2	Amplitude-reflection coefficient	$\beta = 0.9$
3	Distances d_{IRS}	$40m$
4	Distances d_{UE1}	$20m$
5	Distances d_{UE2}	$30m$
6	Path-loss exponents $\alpha_{G_{IRS}}$	2.5
7	Path-loss exponents $\alpha_{g_{UE1}}$	2.5
8	Path-loss exponents $\alpha_{G_{UE2}}$	2.5
9	Target data-rates for the fixed-rate transmission	$\gamma_{th} = 0.1$
10	Number of points for CG-GL	$L = 100$

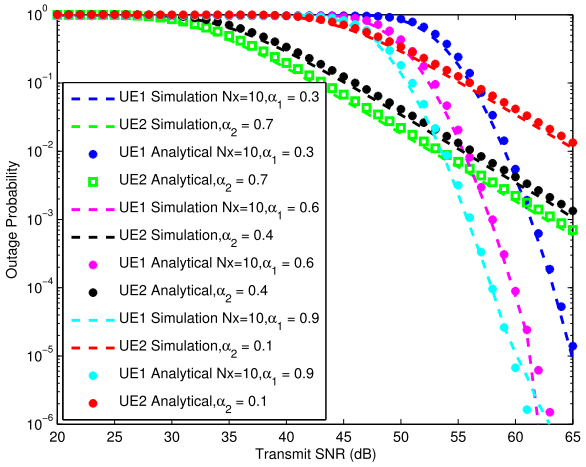

FIGURE 5. OPs of UEs with different power allocation factors.

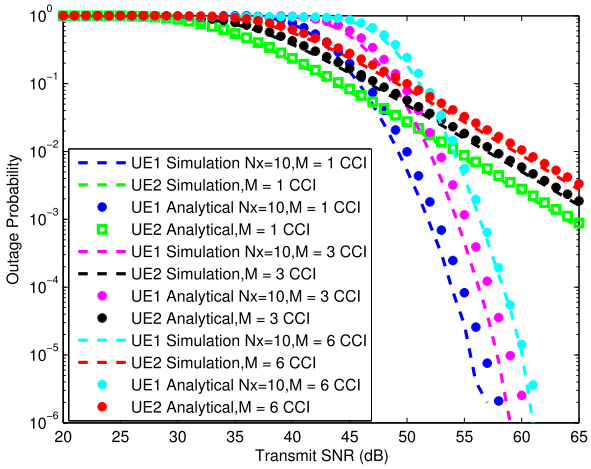

FIGURE 6. OPs of UEs with different number of CCI elements.

that the distance loss coefficients for the CCI noises are the same and equal to 1. The simulation results show that the simulation and analysis results are consistent. That has proved the accuracy of the theory that we built. From the simulation results, we can see that when the number of IRS reflectors changes, the OPs of UE1 change significantly. Specifically, a small OP value corresponds to a small SNR when the number of IRS reflectors is large. In addition, the OP slope of UE1 is much larger than the slope of UE2, which proves the performance of IRS-NOMA network is better than many NOMA networks.

In Fig. 5, we examine the OPs of the UEs in some settings. In which, the power allocation factor of NOMA is 0.3, 0.6 and 0.9 for UE1 and 0.7, 0.4 and 0.1 for UE2 respectively. In this mode, the IRS reflecting element is 10 elements. At UE1 and UE2 are affected by six CCI sources. In this case, we also assume that the distance attenuation coefficient of the CCI term is the same and equal to 1, the power of the CCI noise equal to 1. The simulation results show that the simulation and analysis results are consistent. The simulation results show that when the power allocation factor of NOMA changes, the OPs of the UEs change significantly. Specifically, a small OP value corresponds to a small SNR when the number of IRS reflectors is large. This proves that the performance of IRS-NOMA and NOMA networks depends greatly on the power allocation factor. In addition, UE1's OPs have a much steeper slope than UE2's OPs, which proves that IRS-NOMA network performance is better than many NOMA networks even when the power allocation factor for IRS-NOMA network is smaller.

In Fig. 6, we simulate the OPs of the UEs. In which, the power allocation factor of NOMA is 0.8 for UE1 and 0.2 for UE2 respectively. In this mode, the IRS meta-surface is 10 elements. At UE1 and UE2 are affected by different number of CCI sources. We also assume that the distance attenuation coefficient of the CCI disturbances is the same and equal to 1, the power of the CCI disturbances equal to 1. The simulation results show that the simulation and analysis results are consistent. From the simulation results, we can see that when the number of impacts on the system changes, the OPs of the UEs change significantly. As can be clearly seen in Figure 6, if the system model is disturbed by a single external terminal with fixed transmit power, the performance curve reaches 10^{-6} at an SNR of about 57 dB. On the other hand, if the number of interfering devices increases to 6, the loss in the coding system will decrease exponentially. Meanwhile, there are still a large number of users achieving diversity order in high SNR mode. This was discussed in [40]. This proves that the performance of IRS-NOMA networks is highly dependent on the amount of CCI interference affecting

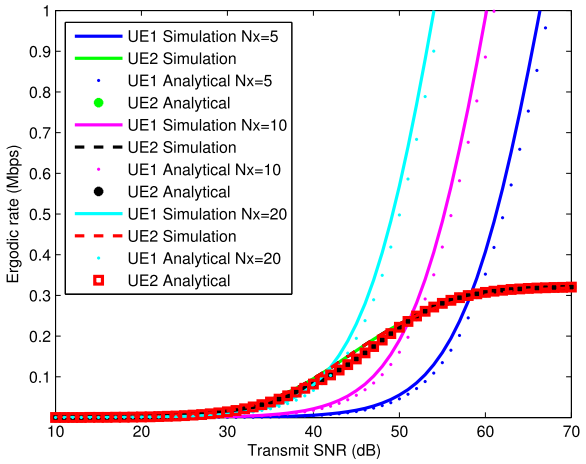

FIGURE 7. ERs of UEs with different IRS reflector numbers.

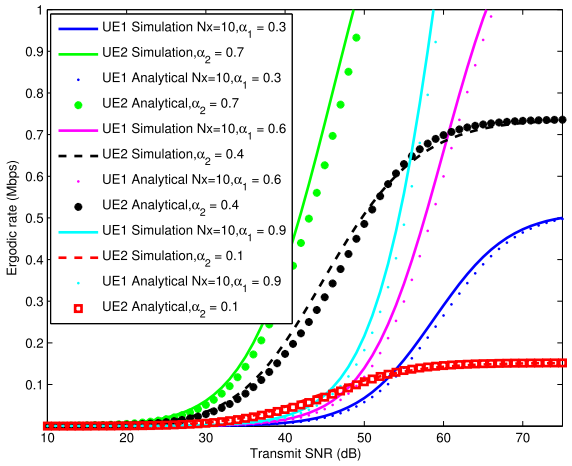

FIGURE 8. ERs of UEs with different power allocation factors.

the system. In addition, the simulation results show that the anti-interference ability of IRS-NOMA network is much better higher transmit SNR.

We simulate Fig. 7 the ERs of UEs in NOMA mode with a power allocation factor of 0.8 for UE1 and 0.2 for UE2, respectively. In this mode, the number of reflector elements of the IRS changes to 5, 10, and 20 reflectors, respectively. At UE1 and UE2 affected by the number of CCI elements is 6 elements. We also assume that the distance attenuation factor of the CCI disturbances is the same and equal to 1, and the power of the CCI disturbances is equal to 1. The results show us that there is a good agreement between simulation and analysis results. From the simulation results, we can see that when the number of IRS reflectors changes, the ERs of UE1 change accordingly. In particular, as the number of IRS elements increases, the ERs achieve larger values with smaller SNRs. This proves that the ER of the IRS-NOMA network with a large number of IRS reflectors is better than the ER of a IRS-NOMA network with a small number of IRS reflectors even when the system is affected by CCI noise. In addition, we find that the ERs of the UEs in the IRS-NOMA network are better than the ERs of the UEs in the NOMA network.

In Fig. 8, we simulate the ERs of UEs in NOMA mode with variable power allocation factors of 0.3, 0.6, 0.9 for UE1 and 0.7, 0.4, respectively. 0.1 for UE2. The UE1 and UE2 affected by the number of CCI sources is 6. We also assume that the distance attenuation factor of the CCI disturbances is the same and equal to 1, and the power of the CCI disturbances is equal to 1. The results show us that there is a good agreement between simulation and analysis results. From the simulation results, we can see that when the NOMA's power allocation factor changes, the ERs of the UEs change accordingly. In particular, as the power allocation factor increases, the ERs of the UEs achieve larger values with smaller SNRs. This proves that the ER of the IRS-NOMA network depends on the power allocation factor even when the system is affected by several levels of CCI.

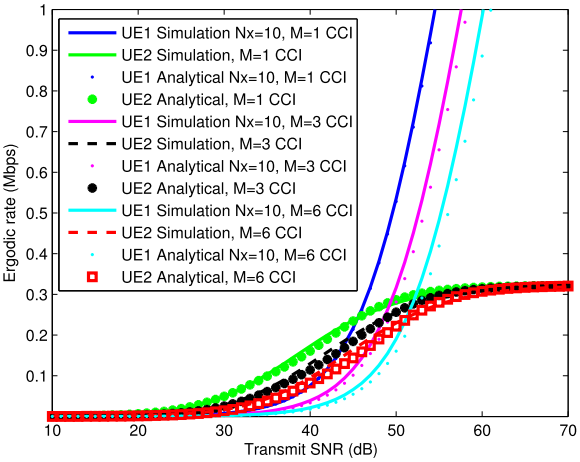

FIGURE 9. ERs of UEs with different number of CCI elements.

We simulate the ERs of UEs in NOMA mode with a power allocation factor of 0.8 for UE1 and 0.2 for UE2, respectively, and all detailed are represented in Fig. 9. In this mode, the IRS reflector number is 10 reflectors. At UE1 and UE2 are affected by the number of CCI sources changing by 1,3, 6 noise elements, respectively. We also assume that the distance attenuation factor of the CCI disturbances is the same and equal to 1, and the power of the CCI disturbances is equal to 1.The results show us that there is a good agreement between simulation and analysis results. From the simulation results, we can see that when the number of CCI noise parts changes, the ERs of the UEs change accordingly. In particular, as the number of CCI fractions increases, the ERs of the UEs achieve smaller values with larger SNRs. This proves that CCI noise has a huge impact on the performance of IRS-NOMA and NOMA networks.

In Fig. 10, we simulate the OPs of the UEs of the IRS-NOMA system and simulate the OPs of the UEs of the IRS-OMA system. In particular, the number of reflection elements of IRS is 5 and 20 elements, respectively. In NOMA mode, the power allocation factor for UE1 is 0.4, UE2

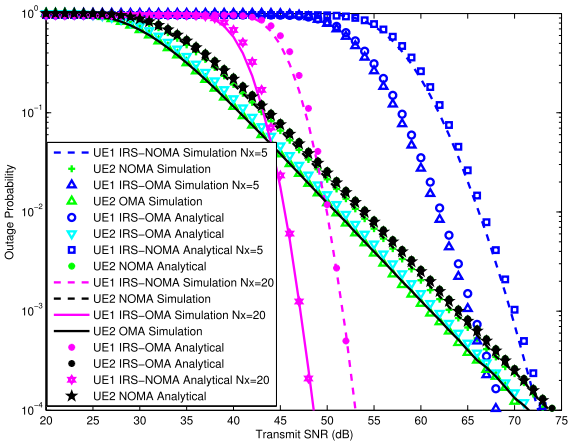

FIGURE 10. Comparison of OPs in the IRS-NOMA system and the IRS-OMA system.

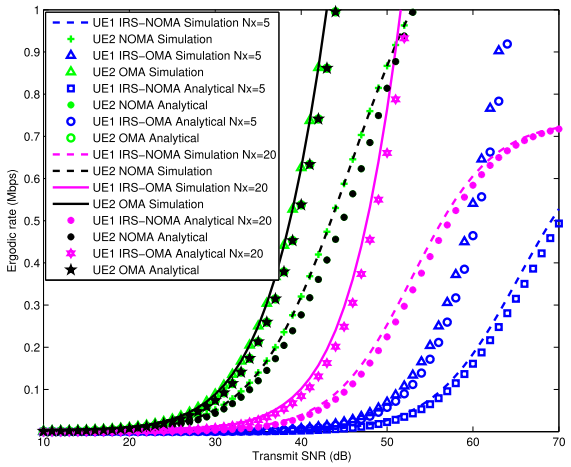

FIGURE 11. Comparison of ERs in the IRS-NOMA system and the IRS-OMA system.

is 0.6. At UE1 and UE2, both systems are affected by 6 CCI disturbances. The simulation results of Fig. 10 show us that in the NOMA system, the NOMA system has higher performance than the OMA system. In addition, we see that in the same system model, the influence of CCI interference on the OPs of UEs in the NOMA system is worse than in the OMA system.

In Fig. 11, we simulate the ERs of the UEs of the IRS-NOMA system and simulate the ERs of the UEs of the IRS-OMA system. In particular, the number of reflection elements of IRS is 5 and 20 elements, respectively. In NOMA mode, the power allocation factor for UE1 is 0.4, UE2 is 0.6. At UE1 and UE2, both systems are affected by 6 CCI disturbances. The simulation results of Fig. 11 show us that in the NOMA system, the NOMA system has higher performance than the OMA system. In addition, we see that in the same system model, the influence of CCI interference on the ERs of UEs in the NOMA system is worse than in the OMA system.

Through simulation results in Figs 10 and 11, we conclude that the performance of IRS-NOMA network and NOMA network that is not supported by IRS depends on the power allocation factors as well as the amount of CCI source affecting on the system. In addition, simulation results have demonstrated that IRS-NOMA network has better CCI immunity than traditional NOMA network, and IRS-NOMA network performance is better than traditional NOMA network.

VI. CONCLUSION

This paper has studied the impact of CCI on users in IRS-NOMA network. In the model we propose the CCI could be independent and identically distributed. We calculated the OPs of the UEs in IRS-NOMA, constructing closed-form expressions of the OPs. In addition, we calculate the ERs of the UEs in IRS-NOMA and in NOMA, construct closed-form expressions of the ERs. To prove the accuracy of the theory, we simulated the OPs of the UEs and the ERs of the UEs in IRS-NOMA. Our analysis and simulation results have proved that the performance of IRS-NOMA is better than IRS-OMA even under CCI interference. Simulation analysis results also demonstrated that IRS-NOMA has better resistance to CCI interference than NOMA which is not supported by IRS. On the other hand, as the number of CCI noise increases, the performance of the network is significantly affected, especially in NOMA networks that are not supported by the IRS. This, once again proves the superiority of the IRS not only to increase the performance of the network, to increase the coverage, but also to be resistant to CCI interference. On the other hand, the results of simulation analysis also prove that changing the power allocation factor in NOMA also greatly affects the performance of the network. The analysis results show that if we allocate NOMA power properly, we can not only increase the performance of the network but also reduce the influence of CCI interference. Furthermore, the design of IRS-NOMA that can be optimized when reinforcement learning can be leveraged as our future research direction.

APPENDIX A
PROOF OF THE PROPOSITION 1

We have:

$$\mathrm{E}[X] = \mathrm{E}\left[\sum_{k=1}^{N_x} \left|G_{IRS,k}\right| \left|g_{UE1,k}\right|\right]. \tag{A.1}$$

According to the expected property (A.1) is rewritten as:

$$\mathrm{E}[X] = \sum_{k=1}^{N_x} \mathrm{E}\left[\left|G_{IRS,k}\right| \left|g_{UE1,k}\right|\right]. \tag{A.2}$$

Since $\left|G_{IRS,k}\right|$ and $\left|g_{UE1,k}\right|$ are independent RVs, (A.2) can be rewritten as

$$\mathrm{E}[X] = \sum_{k=1}^{N_x} \mathrm{E}\left[\left|G_{IRS,k}\right|\right] E\left[\left|g_{UE1,k}\right|\right]. \tag{A.3}$$

On the other hand, $|G_{IRS,k}|$ and $|g_{UE1,k}|$ have variance of 1, so $\mathrm{E}\left[|G_{IRS,k}|\right] = E\left[|g_{UE1,k}|\right] = \sqrt{\frac{\pi}{2}}$, Inferred

$$\mathrm{E}[X] = \sum_{k=1}^{N_x} \frac{\pi}{2} = \frac{N_x \pi}{2}. \tag{A.4}$$

On the other hand:

$$Var[X] = \mathrm{E}\left[(X - E[X])^2\right]. \tag{A.5}$$

Similar to the calculation above, we can easily find

$$Var[X] = N_x \left(1 - \frac{\pi^2}{16}\right). \tag{A.6}$$

The proof of Proposition 1 is completed.

APPENDIX B
PROOF OF THE PROPOSITION 2

We have:

$$F_{\gamma_S}(y) = Pr[\gamma_S < y]. \tag{B.1}$$

Transforming (B.1) we get (B.2)

$$F_{\gamma_S}(y) = Pr\left[X^2 < \frac{y}{n}\right]. \tag{B.2}$$

Transforming (B.2) we get (B.3)

$$F_{\gamma_S}(y) = Pr\left[X < \sqrt{\frac{y}{n}}\right]. \tag{B.3}$$

Transforming (B.3) we get (B.4)

$$F_{\gamma_S}(y) = F_X\left(\sqrt{\frac{y}{n}}\right). \tag{B.4}$$

Then, we have

$$F_{\gamma_S}(y) = \frac{\gamma\left(a+1, \frac{1}{b}\sqrt{\frac{y}{n}}\right)}{\Gamma(a+1)}. \tag{B.5}$$

Move on other way, we have

$$\begin{aligned} f_{\gamma_S}(y) &= \left(F_{\gamma_S}(y)\right)' \\ &= \frac{y^{\frac{a-1}{2}}}{2b^{a+1}\Gamma(a+1)\, n^{\frac{a+1}{2}}} exp\left(-\frac{1}{b}\sqrt{\frac{y}{n}}\right). \end{aligned} \tag{B.6}$$

The proof of Proposition 2 is completed.

APPENDIX C
PROOF OF THE PROPOSITION 3

We have:

$$E[\gamma_S] = n\int_0^\infty x^2 f_X(x)\, dx. \tag{C.1}$$

Substituting (8) into (C.1) we have

$$E[\gamma_S] = \frac{n}{b^{a+1}\Gamma(a+1)} \int_0^\infty x^{a+2} exp\left(-\frac{x}{b}\right) dx. \tag{C.2}$$

By using [27, eq.3.381 (4)], (C.2) can be written in the closed form as

$$E[\gamma_S] = \frac{\Gamma(a+3)\, b^2 n P_S}{\Gamma(a+1)}. \tag{C.3}$$

Other way

$$E\left[\gamma_S^2\right] = \int_0^\infty y^2 f_{\gamma_S}(y)\, dy. \tag{C.4}$$

Substituting (12) into (C.4) we have

$$E\left[\gamma_S^2\right] = \frac{\int_0^\infty y^{\frac{a+3}{2}} exp\left(-\frac{1}{b}\sqrt{\frac{y}{n}}\right) dy}{2b^{a+1}\Gamma(a+1)\, n^{\frac{a+1}{2}}}. \tag{C.5}$$

Set $z = \sqrt{y}$, deduce $2zdz = dy$

$$E\left[\gamma_S^2\right] = \frac{\int_0^\infty z^{a+4} exp\left(-\frac{z}{b\sqrt{n}}\right) dz}{b^{a+1}\Gamma(a+1)\, n^{\frac{a+1}{2}}}. \tag{C.6}$$

By using [27], eq 3.381 (4), (C.6) can be written in the closed form as

$$E\left[\gamma_S^2\right] = \frac{\left(b\sqrt{n}\right)^{a+5}\Gamma(a+5)}{b^{a+1}\Gamma(a+1)\, n^{\frac{a+1}{2}}} = \frac{b^4 n^2 \Gamma(a+5)}{\Gamma(a+1)}. \tag{C.7}$$

The proof of Proposition 3 is completed.

APPENDIX D
PROOF OF THE PROPOSITION 4

We have:

$$F_{\gamma_U}(y) = Pr[\gamma_U < y]. \tag{D.1}$$

Inferred

$$F_{\gamma_U}(y) = Pr\left[|G_{UE2}|^2 < \frac{y}{m}\right]. \tag{D.2}$$

Transforming (D.2) we get (D.3)

$$F_{\gamma_U}(y) = Pr\left[|G_{UE2}| < \sqrt{\frac{y}{m}}\right]. \tag{D.3}$$

According to the inferred probability theory

$$F_{\gamma_U}(y) = F_{G_{UE2}}\left(\sqrt{\frac{y}{m}}\right). \tag{D.4}$$

Since, $|G_{UE2}|$ is a random variable with RV distribution, we have the CDF of γ_U:

$$F_{\gamma_U}(y) = 1 - exp\left(-\frac{y}{2m}\right). \tag{D.5}$$

In other way, we have

$$f_{\gamma_U}(y) = \left(F_{\gamma_U}(y)\right)' = \frac{1}{2m} exp\left(-\frac{y}{2m}\right). \tag{D.6}$$

The proof of Proposition 4 is completed.

APPENDIX E
PROOF OF PROPOSITION 5

We have:

$$E\left[\gamma_U\right] = \int_0^\infty y f_{\gamma_U}(y)\, dy. \tag{E.1}$$

Substituting (16) into (E.1) we have

$$E\left[\gamma_U\right] = \frac{1}{2m}\int_0^\infty y.exp\left(-\frac{y}{2m}\right) dy. \tag{E.2}$$

By using [27, eq 3.351 (3)], (E.2) can be written in the closed form as

$$E\left[\gamma_U\right] = \frac{1}{2m}\left(\frac{1}{2m}\right)^{-2} = 2m. \tag{E.3}$$

In other way, $E\left[\gamma_U^2\right]$ is expressed by

$$E\left[\gamma_U^2\right] = \frac{1}{2m}\int_0^\infty y^2 exp\left(-\frac{y}{2m}\right) dy. \tag{E.4}$$

By using [27, eq 3.351 (3)], (E.4) can be written in the closed form as

$$E\left[\gamma_U^2\right] = 2!(2m)^2. \tag{E.5}$$

The proof of Proposition 5 is completed.

APPENDIX F
PROOF OF PROPOSITION 6

We have:

$$E\left[\gamma_I\right] = \int_0^\infty y f_{\gamma_I}(y)\, dy. \tag{F.1}$$

Substituting (1) into (F.1) we have

$$E\left[\gamma_I\right] = \frac{\int_0^\infty y^M exp\left(\frac{-y}{P_I\Omega_I}\right) dy}{(P_I\Omega_I)^M (M-1)!}. \tag{F.2}$$

By using [27, eq 3.351 (3)], (F.2) can be written in the closed form as

$$E\left[\gamma_I\right] = MP_I\Omega_I. \tag{F.3}$$

In other way, $E\left[\gamma_I^2\right]$ is given by

$$E\left[\gamma_I^2\right] = \int_0^\infty y^2 f_{\gamma_I}(y)\, dy. \tag{F.4}$$

Substituting (1) into (F.4) we have

$$E\left[\gamma_I^2\right] = \frac{\int_0^\infty y^{M+1} exp\left(\frac{-y}{P_I\Omega_I}\right) dy}{(P_I\Omega_I)^M (M-1)!}. \tag{F.5}$$

By using [27, eq 3.351 (3)], (F.5) can be written in the closed form as

$$E\left[\gamma_I^2\right] = M(M+1)(P_I\Omega_I)^2. \tag{F.6}$$

The proof of Proposition 6 is completed.

APPENDIX G
PROOF OF PROPOSITION 7

We have:

$$OP_{UE1}^{\infty} = \int_0^\infty \frac{\left(\frac{1}{b}\sqrt{\frac{\gamma_{th}(y+1)}{(\alpha_1-\gamma_{th}\alpha_2)n}}\right)^{a+1} y^{M-1} exp\left(\frac{-y}{P_I\Omega_I}\right) \mathrm{dy}}{\Gamma(a+1)(P_I\Omega_I)^M (M-1)!}. \tag{G.1}$$

Transforming (G1) we have

$$OP_{UE1}^{\infty} = \frac{\left(\frac{1}{b}\sqrt{\frac{\gamma_{th}}{(\alpha_1-\gamma_{th}\alpha_2)n}}\right)^{a+1} M_1}{\Gamma(a+1)(P_I\Omega_I)^M (M-1)!}. \tag{G.2}$$

where M_1 is

$$M_1 = \int_0^\infty (y+1)^{\frac{a+1}{2}} y^{M-1} exp\left(\frac{-y}{P_I\Omega_I}\right) \mathrm{dy}. \tag{G.3}$$

We calculate M_1 as follows Let $z = y+1$, $dz = dy$

$$M_1 = \int_1^\infty z^{\frac{a+1}{2}} (z-1)^{M-1} exp\left(\frac{-z+1}{P_I\Omega_I}\right) \mathrm{dz}. \tag{G.4}$$

Transforming (G4) we get (G5)

$$M_1 = exp\left(\frac{1}{P_I\Omega_I}\right)\int_1^\infty z^{\frac{a+1}{2}} (z-1)^{M-1} exp\left(\frac{-z}{P_I\Omega_I}\right) \mathrm{dz}. \tag{G.5}$$

$$M_1 = exp\left(\frac{1}{P_I\Omega_I}\right) M_2. \tag{G.6}$$

where M_2 is

$$M_2 = \int_1^\infty z^{\frac{a+1}{2}} (z-1)^{M-1} exp\left(\frac{-z}{P_I\Omega_I}\right) \mathrm{dz}. \tag{G.7}$$

We calculate M_2 as follows

$$M_2 = \int_1^\infty z^{\frac{a+1}{2}} \sum_{j=0}^{M-1} C_{M-1}^j z^{M-1-j}(-1)^j exp\left(\frac{-z}{P_I\Omega_I}\right) \mathrm{dz} \tag{G.8}$$

Transforming (G8) we get (G9)

$$M_2 = (-1)^j \sum_{j=0}^{M-1} C_{M-1}^j \int_1^\infty z^{\frac{a+1}{2}+M-j-1} exp\left(\frac{-z}{P_I\Omega_I}\right) \mathrm{dz} \tag{G.9}$$

Set $e = \frac{a+1}{2} + M$

$$M_2 = (-1)^j \sum_{j=0}^{M-1} C_{M-1}^j \int_1^\infty z^{e-j-1} exp\left(\frac{-z}{P_I\Omega_I}\right) \mathrm{dz} \tag{G.10}$$

Appling the formula in [[27], eq 3.381(3)], M_2 is rewritten as

$$M_2 = (-1)^j \sum_{j=0}^{M-1} \left[C_{M-1}^{j} \left(\frac{1}{P_I \Omega_I} \right)^{-(e-j)} \Gamma\left(e-j, \frac{1}{P_I \Omega_I} \right) \right] \tag{G.11}$$

Substituting M_2 into M_1 and replacing M_1 into $G2$ we have

$$OP_{UE1}^{\infty} = \frac{\left(\frac{1}{b} \sqrt{\frac{\gamma_{th}}{(\alpha_1 - \gamma_{th}\alpha_2)n}} \right)^{a+1} exp\left(\frac{1}{P_I \Omega_I} \right)}{\Gamma(a+1) (P_I \Omega_I)^M (M-1)!} M_2 \tag{G.12}$$

The proof of Proposition 7 is completed.

APPENDIX H
PROOF OF PROPOSITION 8

We have

$$OP_{UE2}^{\infty} = \int_0^{\infty} \left(\frac{\gamma_{th}(y+1)}{2m(\alpha_2 - \gamma_{th}\alpha_1)} \right) f_{\gamma_I}(y)\, dy. \tag{H.1}$$

At this step, (H.1) is equivalent to (H.2)

$$OP_{UE2}^{\infty} = \frac{\gamma_{th} \int_0^{\infty} (y+1) y^{M-1} exp\left(\frac{-y}{P_I \Omega_I} \right) dy}{2m(\alpha_2 - \gamma_{th}\alpha_1) (P_I \Omega_I)^M (M-1)!}. \tag{H.2}$$

Transforming (H. 2) we get (H. 3)

$$OP_{UE2}^{\infty} = \frac{\gamma_{th} \left[\int_0^{\infty} y^M exp\left(\frac{-y}{P_I \Omega_I} \right) dy + \int_0^{\infty} y^{M-1} exp\left(\frac{-y}{P_I \Omega_I} \right) dy \right]}{2m(\alpha_2 - \gamma_{th}\alpha_1) (P_I \Omega_I)^M (M-1)!} \tag{H.3}$$

By using the formula in [[27], eq 3.351(3)], OP_{UE2}^{∞} is expressed by

$$OP_{UE2}^{\infty} = \frac{\gamma_{th} \left[M(M+1) (P_I \Omega_I)^2 + 1 \right]}{2m(\alpha_2 - \gamma_{th}\alpha_1)}. \tag{H.4}$$

The proof of Proposition 8 is completed.

REFERENCES

[1] D. Sarkar, S. S. Yadav, V. Pal, N. Kumar, and S. K. Patra, "A comprehensive survey on IRS-assisted NOMA-based 6G wireless network: Design perspectives, challenges and future directions," *IEEE Trans. Netw. Service Manage.*, vol. 21, no. 2, pp. 2539–2562, Apr. 2024.

[2] T.-A. Nguyen, H.-V. Nguyen, D.-T. Do, and A. Silva, "Performance analysis of downlink double-IRS systems relying on non-orthogonal multiple access," *IEEE Access*, vol. 11, pp. 110208–110220, 2023.

[3] H. Amiriara, F. Ashtiani, M. Mirmohseni, and M. Nasiri-Kenari, "IRS-user association in IRS-aided MISO wireless networks: Convex optimization and machine learning approaches," *IEEE Trans. Veh. Technol.*, vol. 72, no. 11, pp. 14305–14316, Nov. 2023.

[4] S. Thushan, S. Ali, N. H. Mahmood, N. Rajatheva, and M. Latva-Aho, "Deep learning-based blind multiple user detection for grant-free SCMA and MUSA systems," *IEEE Trans. Mach. Learn. Commun. Netw.*, vol. 1, pp. 61–77, 2023.

[5] D.-T. Do, C.-B. Le, A. Vahid, and S. Mumtaz, "Antenna selection and device grouping for spectrum-efficient UAV-assisted IoT systems," *IEEE Internet Things J.*, vol. 10, no. 9, pp. 8014–8030, May 2023.

[6] M.-S. Van Nguyen, D.-T. Do, A. Vahid, S. Muhaidat, and D. Sicker, "Enhancing NOMA backscatter IoT communications with RIS," *IEEE Internet Things J.*, vol. 11, no. 4, pp. 5604–5622, Feb. 2024.

[7] D. Zhang, Y. Liu, Z. Ding, Z. Zhou, A. Nallanathan, and T. Sato, "Performance analysis of non-regenerative massive-MIMO-NOMA relay systems for 5G," *IEEE Trans. Commun.*, vol. 65, no. 11, pp. 4777–4790, Nov. 2017, doi: 10.1109/TCOMM.2017.2739728.

[8] M.-S. Van Nguyen, D.-T. Do, S. Al-Rubaye, S. Mumtaz, A. Al-Dulaimi, and O. A. Dobre, "Exploiting impacts of antenna selection and energy harvesting for massive network connectivity," *IEEE Trans. Commun.*, vol. 69, no. 11, pp. 7587–7602, Nov. 2021.

[9] D. Bepari, S. Mondal, A. Chandra, R. Shukla, Y. Liu, M. Guizani, and A. Nallanathan, "A survey on applications of cache-aided NOMA," *IEEE Commun. Surveys Tuts.*, vol. 25, no. 3, pp. 1571–1603, 3rd Quart., 2023.

[10] H. Al-Obiedollah, H. B. Salameh, K. Cumanan, Z. Ding, and O. A. Dobre, "Competitive IRS assignment for IRS-based NOMA system," *IEEE Wireless Commun. Lett.*, vol. 13, no. 2, pp. 505–509, Feb. 2024.

[11] S. Pakravan, J.-Y. Chouinard, X. Li, M. Zeng, W. Hao, Q.-V. Pham, and O. A. Dobre, "Physical layer security for NOMA systems: Requirements, issues, and recommendations," *IEEE Internet Things J.*, vol. 10, no. 24, pp. 21721–21737, Dec. 2023.

[12] S. Almaghthawi, E. Alsusa, and A. Al-Dweik, "On the performance of IRS-aided NOMA in interference-limited networks," *IEEE Wireless Commun. Lett.*, vol. 13, no. 2, pp. 560–564, Feb. 2024.

[13] V. Ozduran, M. Mohammadi, N. Nomikos, I. S. Ansari, and P. Trakadas, "On the performance of uplink power-domain NOMA with imperfect CSI and SIC in 6G networks," TechRxiv, Oct. 2023, doi: 10.36227/techrxiv.24138750.v2.

[14] V. Ozduran, N. Nomikos, E. Soleimani, I. S. Ansari, and P. Trakadas, "Relay-aided uplink NOMA under non-orthogonal CCI and imperfect SIC in 6G networks," TechRxiv, Nov. 2023, doi: 10.36227/techrxiv.24523801.v1.

[15] H.-M. Wang, J. Bai, and L. Dong, "Intelligent reflecting surfaces assisted secure transmission without Eavesdropper's CSI," *IEEE Signal Process. Lett.*, vol. 27, pp. 1300–1304, 2020.

[16] Y. Cai, M.-M. Zhao, K. Xu, and R. Zhang, "Intelligent reflecting surface aided full-duplex communication: Passive beamforming and deployment design," *IEEE Trans. Wireless Commun.*, vol. 21, no. 1, pp. 383–397, Jan. 2022.

[17] X. Pang, W. Mei, N. Zhao, and R. Zhang, "Intelligent reflecting surface assisted interference mitigation for cellular-connected UAV," *IEEE Wireless Commun. Lett.*, vol. 11, no. 8, pp. 1708–1712, Aug. 2022.

[18] B. Zheng, Q. Wu, and R. Zhang, "Intelligent reflecting surface-assisted multiple access with user pairing: NOMA or OMA?" *IEEE Commun. Lett.*, vol. 24, no. 4, pp. 753–757, Apr. 2020.

[19] Z. Zhang, J. Chen, Q. Wu, Y. Liu, L. Lv, and X. Su, "Securing NOMA networks by exploiting intelligent reflecting surface," *IEEE Trans. Commun.*, vol. 70, no. 2, pp. 1096–1111, Feb. 2022.

[20] Z. Tang, T. Hou, Y. Liu, J. Zhang, and L. Hanzo, "Physical layer security of intelligent reflective surface aided NOMA networks," *IEEE Trans. Veh. Technol.*, vol. 71, no. 7, pp. 7821–7834, Jul. 2022.

[21] Z. Zhang, J. Chen, Q. Wu, Y. Liu, L. Lv, and X. Su, "Enhancing security of NOMA networks via distributed intelligent reflecting surfaces," in *Proc. IEEE Global Commun. Conf. (GLOBECOM)*, Dec. 2021, pp. 1–6.

[22] A. Papoulis and U. Pillai, *Probability, Random Variables and Stochastic Processes*, vol. 11. New York, NY, USA: McGraw-Hill, 2001.

[23] V. Ozduran and N. Nomikos, "On the leakage-rate performance of untrusted relay-aided NOMA under co-channel interference," *Telecommun. Syst.*, vol. 85, pp. 67–86, Nov. 2024, doi: 10.1007/s11235-023-01071-9.

[24] V. Ozduran, "Leakage rate analysis with imperfect channel state information for cooperative nonorthogonal multiple access networks," *Int. J. Commun. Syst.*, vol. 33, p. e4387, Jun. 2020, doi: 10.1002/dac.4387.

[25] M. V. Jamali and H. Mahdavifar, "Uplink non-orthogonal multiple access over mixed RF-FSO systems," *IEEE Trans. Wireless Commun.*, vol. 19, no. 5, pp. 3558–3574, May 2020.

[26] S. Primak, V. Kontorovich, and V. Lyandres, *Stochastic Methods and Their Applications to Communications Stochastic Differential Equations Approach*. West Sussex, U.K.: Wiley, 2004.

[27] I. S. Gradshteyn and I. M. Ryzhik, *Table of Integrals, Series, and Products*, 6th ed. New York, NY, USA: Academic, 2000.

[28] D. da Costa and S. Aissa, "Capacity analysis of cooperative systems with relay selection in Nakagami-*m* fading," *IEEE Commun. Lett.*, vol. 13, no. 9, pp. 637–639, Sep. 2009.
[29] V. Ozduran, M. Mohammadi, I. S. Ansari, and N. Nomikos, "Performance analysis of uplink non-orthogonal multiple access in the presence of co-channel interference," *IEEE Trans. Veh. Technol.*, vol. 72, no. 9, pp. 11590–11602, Sep. 2023.
[30] V. Ozduran, "Co-channel interference effects on downlink power-domain non-orthogonal multiple access," *Wireless Pers. Commun.*, vol. 122, pp. 1153–1170, Aug. 2022.
[31] R. Jain, A. Trivedi, and A. Gupta, "Co-channel interference suppression for cellular-connected UAV using NOMA," in *Proc. IEEE 4th Conf. Inf. Commun. Technol. (CICT)*, Chennai, India, Dec. 2020, pp. 1–6, doi: 10.1109/CICT51604.2020.9312102.
[32] S. Xie, B. Zhang, D. Guo, R. Xu, C. Li, and W. Ma, "Performance analysis of non-orthogonal multiple access with co-channel interference in a satellite communication system," in *Proc. 11th Int. Conf. Wireless Commun. Signal Process. (WCSP)*, Xi'an, China, Oct. 2019, pp. 1–6, doi: 10.1109/WCSP.2019.8927990.
[33] E. Basar, M. Di Renzo, J. De Rosny, M. Debbah, M.-S. Alouini, and R. Zhang, "Wireless communications through reconfigurable intelligent surfaces," *IEEE Access*, vol. 7, pp. 116753–116773, 2019.
[34] C. Huang, A. Zappone, G. C. Alexandropoulos, M. Debbah, and C. Yuen, "Reconfigurable intelligent surfaces for energy efficiency in wireless communication," *IEEE Trans. Wireless Commun.*, vol. 18, no. 8, pp. 4157–4170, Aug. 2019.
[35] H. Zhang, B. Di, L. Song, and Z. Han, "Reconfigurable intelligent surfaces assisted communications with limited phase shifts: How many phase shifts are enough?" *IEEE Trans. Veh. Technol.*, vol. 69, no. 4, pp. 4498–4502, Apr. 2020.
[36] Z. Ding, P. Fan, and H. V. Poor, "Impact of user pairing on 5G nonorthogonal multiple-access downlink transmissions," *IEEE Trans. Veh. Technol.*, vol. 65, no. 8, pp. 6010–6023, Aug. 2016.
[37] Y. Fu, M. Zhang, L. Salaün, C. W. Sung, and C. S. Chen, "Zero-forcing oriented power minimization for multi-cell MISO-NOMA systems: A joint user grouping, beamforming, and power control perspective," *IEEE J. Sel. Areas Commun.*, vol. 38, no. 8, pp. 1925–1940, Aug. 2020.
[38] J. C. Maxwell, "5G NR user equipment (UE) radio transmission and reception; part 1: Range 1 standalone release 15 V. 15.2. 0 document 3GPP TS 38.101-1," in *A Treatise on Electricity and Magnetism*, vol. 2. Oxford, U.K.: Clarendon, 2018, pp. 68–73.
[39] Y. Cheng, K. H. Li, Y. Liu, K. C. Teh, and H. Vincent Poor, "Downlink and uplink intelligent reflecting surface aided networks: NOMA and OMA," *IEEE Trans. Wireless Commun.*, vol. 20, no. 6, pp. 3988–4000, Jun. 2021.
[40] V. Ozduran and S. B. Yarman, "Impact of the external co-channel interferences over multiuser bi-directional wireless relaying networks—Part I: System description and outage analysis," *Wireless Pers. Commun.*, vol. 78, pp. 1277–1295, May 2014, doi: 10.1007/s11277-014-1817-9.

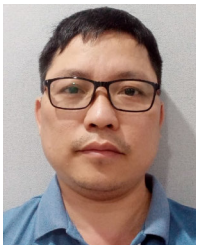

THAI-ANH NGUYEN was born in Vietnam. He received the degree in electrical and electronic engineering from Vietnam Military Technical Academy, in 2009, and the master's degree from the Ho Chi Minh University of Technology and Education, Vietnam, in 2018, with a major in electronics and telecommunications. He is currently pursuing the Ph.D. degree with the Industrial University of Ho Chi Minh City, Vietnam. From 2009 to 2023, he was a Lecturer with the Naval Technical College, Vietnam. His research interest includes the applications of intelligent reflective surfaces in communications networks.

HOANG-VIET NGUYEN was born in Ho Chi Minh City, Vietnam, in 1978. He received the master's degree in optical communications from Osaka Prefecture University, Osaka, Japan, in June 2004, and the Ph.D. degree in optical communications from Hunan University, Changsha, China, in 2015. Since 2007, he has been a Lecturer with the Industrial University of Ho Chi Minh City, Ho Chi Minh City. His current research interests include high-speed optical communication, wavelength division multiplexing, radio over fiber, cognitive radio, and satellite communication.

DINH-THUAN DO (Senior Member, IEEE) received the M.Sc. and Ph.D. degrees in electrical engineering from Vietnam National University, Ho Chi Minh City (VNU-HCM), in 2007 and 2012, respectively. Prior to joining academia, he was a Senior Engineer with the Telecommunications Industry, VinaPhone Mobile Network (the biggest cellular network provider in Vietnam), from 2003 to 2009. Before to joining the University of Mount Union, he was a Research Scientist with the University of Colorado Denver, in 2022, and The University of Texas at Austin, in 2021; and as an Assistant Professor with Asia University, Taiwan, from 2020 to 2021. His publications include more than 120 SCIE/SCI-indexed journal articles, five edited books (IET, Springer), and more than 50 international conference papers. He was a recipient of the 2015 Golden Globe Award by Vietnamese Ministry of Science and Technology (top ten outstanding scientists nationwide). He also received the Medal of Creative Young Talents, in 2015. He was named in the top 14 highly cited scientists at Asia University, in 2021 (Stanford's list of top 2% scientists in the world, October 2020, October 2021, October 2022, and October 2023). He is currently serving as an Associate Editor for IEEE TRANSACTION ON VEHICULAR TECHNOLOGY and *Computer Communications* (Elsevier). He has also served as the Lead Guest Editor/the Guest Editor for more than 20 special issues of journals, such as *Physical Communication* (Elsevier) and *Annals of Telecommunications* (Elsevier).

BYUNG MOO LEE (Senior Member, IEEE) received the Ph.D. degree in electrical and computer engineering from the University of California at Irvine, Irvine, CA, USA, in 2006.

He is currently an Associate Professor with the Department of Intelligent Mechatronics Engineering, Sejong University, Seoul, South Korea. Prior to joining Sejong University, he had ten years of industry experience, including research positions with the Samsung Electronics Seoul Research and Development Center, the Samsung Advanced Institute of Technology (SAIT), and Korea Telecom (KT) Research and Development Center. During his industry experience, he participated in IEEE 802.16/11, Wi-Fi Alliance, and 3GPP LTE standardizations, and also participated in Mobile VCE and Green Touch Research Consortiums, where he made numerous contributions and filed a number of related patents. His research interests include wireless communications, signal processing, and machine learning applications. He served as the Vice Chairperson for the Wi-Fi Alliance Display MTG, from 2015 to 2016.